A unified view of imaging the elastic properties of tissue

Kevin J. Parker, Lawrence S. Taylor, and Sheryl Gracewski
School of Engineering and Applied Sciences, University of Rochester, P.O. Box 270126, Rochester, New York 14627-0127

Deborah J. Rubens
Department of Radiology, University of Rochester Medical Center, 601 Elmwood Avenue, Rochester, New York 14642-8648

(Received 8 April 2004; revised 24 January 2005; accepted 28 January 2005)

A number of different approaches have been developed to estimate and image the elastic properties of tissue. The biomechanical properties of tissues are vitally linked to function and pathology, but cannot be directly assessed by conventional ultrasound, MRI, CT, or nuclear imaging. Research developments have introduced new approaches, using either MRI or ultrasound to image the tissue response to some stimulus. A wide range of stimuli has been evaluated, including heat, water jets, vibration shear waves, compression, and quasistatic compression, using single or multiple steps or low-frequency (<10 Hz) cyclic excitation. These may seem to be greatly dissimilar, and appear to produce distinctly different types of information and images. However, our purpose in this tutorial is to review the major classes of excitation stimuli, and then to demonstrate that they produce responses that fall within a common spectrum of elastic behavior. Within this spectrum, the major classes of excitation include step compression, cyclic quasistatic compression, harmonic shear wave excitation, and transient shear wave excitation. The information they reveal about the unknown elastic distribution within an imaging region of interest are shown to be fundamentally related because the tissue responses are governed by the same equation. Examples use simple geometry to emphasize the common nature of the approaches.
[DOI: 10.1121/1.1880772]

PACS numbers: 43.80.Qf, 43.80.Ev, 43.80.Jz [FD] Pages: 2705–2712

I. INTRODUCTION

The biomechanical properties of tissues, particularly the stiffness or tactile hardness of tissues, are inextricably linked to the function, the composition, and the relative state of the tissue with respect to inflammation or pathology.[1] Thus, a number of approaches have been proposed to develop estimates of *in vivo* tissue elasticity. Significant among these in the late 1980s were Krouskop *et al.*, using an M-mode Doppler analysis of muscle tissue during externally applied vibration,[2] and Sato *et al.*, using full B-scan imaging of muscle during vibration to follow the propagating shear waves and thus make a regional estimate of Young's modulus (E).[3] The milestone of creating an actual image of a region of interest, demonstrating the detection of a region of high stiffness, surrounded by softer material, was reached in 1988.[4] This was extended to real-time imaging using slightly modified color Doppler scanning to image a vibration field, and finite element models were employed to demonstrate the sonoelastic void produced by a relatively hard abnormality in an otherwise soft background material that contains a propagating shear wave.[5,6] These general results were later refined and applied to a variety of anatomical and clinical tasks[7] along with expansions of the theoretical basis for vibration sonoelastography.[8,9] Meanwhile, Levinson, who had collaborated with Krouskop and Sato on the key muscle elasticity experiments, applied a number of vibrational and quasistatic techniques to create localized estimates of muscle elasticity, even during active contraction.[10,11] Independently, Ophir and colleagues developed an approach in which tissue was imaged before and after a step compression[12,13] to determine local estimates of strain. Strain imaging of tissue proved to be capable of displaying the relative responses of hard and soft regions at high resolution.[14,15]

Compression can be applied as a single step or as a series of steps.[16] Additional techniques include single-step shear[17] and cyclical, quasistatic harmonic excitation[18] with frequencies on the order of 5–10 Hz.[19]

Magnetic resonance imaging has also been combined with shear wave excitation to perform magnetic resonance elastography (MRE).[20–23] Inverse solutions have been applied to the three-dimensional vector displacement field available in MRE experiments to solve for unknown local elastic parameters.

Another approach is to use a transient tone burst of shear wave excitation, instead of steady-state excitation.[24,25] The excitation stimuli can also be provided directly by acoustic radiation force (ARF) from the ultrasound itself,[26,27] which can be used to create transient[28,29] or harmonic tissue displacements.[30,31] Together, these different approaches provide a diverse and creative set of stimuli that produce measurable changes in tissue. We seek to understand any commonality that may exist among the set of approaches.

In the next sections, we examine a simple homogeneous isotropic linear viscoelastic material under excitation by a progressive set of displacements: compression, shear, quasistatic cyclic shear, and vibration. The material is considered with and without a small inclusion that has a slightly elevated Young's modulus (E) with respect to the surrounding

material. It is shown that the elastic response within the material under the different stimuli all belong within a common spectrum of elastic behavior, and some information concerning the inclusion can be derived from each of the responses to the stimuli.

II. OVERVIEW OF GOVERNING EQUATIONS

Following the methods of continuum mechanics, the governing equations for a deformable medium can be obtained by applying, to any part of the medium, conservation of linear momentum, given by

$$\frac{d}{dt}\int_V\int\int \rho\dot{\mathbf{u}}\,dV=\int_S\int\mathbf{T}^{(\mathbf{n})}\,dS+\int_V\int\int\rho\mathbf{b}\,dV. \quad (1)$$

This equation states that the rate of change of linear momentum is equal to the resultant applied surface and body forces. In this equation, ρ is the density, $\mathbf{u}$ is the displacement vector (with the superposed dot indicating a time derivative), $\mathbf{b}$ is the body force per unit mass vector, and $\mathbf{T}^{(\mathbf{n})}$ is the traction vector on the surface S (with outward unit normal $\mathbf{n}$) of volume V.

Writing the traction vector in terms of the stress tensor σ as

$$\mathbf{T}^{(\mathbf{n})}=\sigma\cdot\mathbf{n}, \quad (2)$$

we can use the divergence theorem to obtain the differential form of conservation of linear momentum,

$$\rho\ddot{\mathbf{u}}=\boldsymbol{\nabla}\cdot\sigma+\rho\mathbf{b}. \quad (3)$$

In measurements of elastic properties, the body forces (such as gravity) are either negligible or their effects can be subtracted from the measured response. Therefore, the last term will not be considered further in this discussion.

To complete the problem statement, the material behavior must be specified. If the deformation is small enough, it can be expressed in terms of the infinitesimal strain tensor,

$$\epsilon_{ij}=\frac{1}{2}\left(\frac{\partial u_i}{\partial x_j}+\frac{\partial u_j}{\partial x_i}\right). \quad (4)$$

Then, the constitutive relation relating stress and strain for a linear-elastic, isotropic medium can be written as

$$\sigma_{ij}=(2\mu\epsilon_{ij}+\lambda\epsilon_{kk}\delta_{ij})=\frac{E}{(1+\nu)}\left(\epsilon_{ij}+\frac{\nu}{1-2\nu}\epsilon_{kk}\delta_{ij}\right), \quad (5)$$

where λ and μ are called the Lamé constants, μ is also the shear modulus, E is the elastic or Young's modulus, and ν is Poisson's ratio. In this equation, the summation convention has been used and δ_{ij} is the Kronecker delta equal to 1 if $i=j$ and 0 otherwise.

In homogeneous regions, where λ and μ are constant, Eqs. (3)–(5) can be combined to obtain an equation in terms of the displacement vector alone as

$$(\lambda+\mu)\frac{\partial^2 u_j}{\partial x_j\,\partial x_i}+\mu\frac{\partial^2 u_i}{\partial x_j\,\partial x_j}=\rho\ddot{u}_i,$$

or

$$(\lambda+\mu)\boldsymbol{\nabla}(\boldsymbol{\nabla}\cdot\mathbf{u})+\mu\,\nabla^2\mathbf{u}=\rho\ddot{\mathbf{u}}, \quad (6)$$

where the body forces, such as gravity, have been assumed negligible. This equation, with given boundary and initial conditions, governs the general dynamic response of a homogeneous, isotropic, linearly elastic material to a force or displacement excitation. If loads are applied slowly (quasistatically) or if the displacement response to a constant load is measured after all the motion has stopped, then the right-hand side of this equation is negligible and set equal to zero. Therefore, this equation governs the static, quasistatic, and dynamic (transient, harmonic, and wave propagation) responses that can occur in response to applied loads.

The lossy nature of biological tissues is often modeled using a viscoelastic model. Such a model can be implemented in these equations for a time-harmonic excitation by assuming that λ and μ are complex. In this case, the wave or vibration amplitude will decay with distance from the excitation point, and the loss will generally increase with increasing frequency. For a more in-depth presentation of the derivation and solution of the elastic and viscoelastic equations, see Kolsky[32] and Achenbach.[33]

At times, it is convenient to represent the response in terms of waves propagating within the tissue. Two types of plane wave, shear waves and pressure waves, propagate independently in the bulk material, interacting only at boundaries. The shear wave equation can easily be obtained from Eq. (6) by noting that there is no volume change as layers of material move in shear, transverse to the direction of propagation, so the dilatation $\boldsymbol{\nabla}\cdot\mathbf{u}=0$. The shear wave equation is then

$$\nabla^2\mathbf{u}=\frac{1}{c_s^2}\ddot{\mathbf{u}}, \quad (7)$$

where the shear wave speed is

$$c_s=\sqrt{\frac{\mu}{\rho}}. \quad (8)$$

This equation can either be solved in terms of standing waves or propagating waves, depending on the particular conditions.

Propagating plane pressure waves are irrotational, that is, $\boldsymbol{\nabla}\times\mathbf{u}=\mathbf{0}$ so $\mathbf{u}$ can be written in terms of a potential as $\mathbf{u}=\boldsymbol{\nabla}\psi$. Using the vector identity $\nabla^2\mathbf{u}=\boldsymbol{\nabla}\boldsymbol{\nabla}\cdot\mathbf{u}-\boldsymbol{\nabla}\times\boldsymbol{\nabla}\times\mathbf{u}$, we can obtain the wave equation for $\boldsymbol{\nabla}\psi$ as

$$\nabla^2(\boldsymbol{\nabla}\psi)=\frac{1}{c_p^2}(\ddot{\boldsymbol{\nabla}\psi}), \quad (9)$$

and the pressure wave speed is

$$c_p=\sqrt{\frac{\lambda+2\mu}{\rho}}. \quad (10)$$

For typical biomaterials, the pressure wave speed is orders of magnitude faster than the shear wave speed. Consistent with this statement, biological tissues are nearly incompressible with $0.49<\nu<0.5$. In the limit, as ν approaches 0.5, the shear modulus $\mu=E/2(1+\nu)\rightarrow E/3$. Therefore, for a nearly incompressible material, a measurement of the shear

wave speed $c_s \approx \sqrt{E/3\rho}$ can be used to obtain information about the stiffness of the material. Therefore, in elastographic imaging experiments, the focus of attention is typically on the shear wave properties and not on pressure wave properties, which have already been investigated extensively in ultrasonic tissue characterization studies.

Equation (6) can also be a starting point for the consideration of step-compression elastography experiments. For static displacement or very low-frequency cyclic motion, the inertial terms are negligibly small. And for nearly incompressible biomaterials, the divergence (or dilatation) $\nabla \cdot \mathbf{u}$ is nearly zero, so Eq. (6) reduces to Laplace's equation,

$$\nabla^2 \mathbf{u} = \mathbf{0}. \tag{11}$$

Solutions to Laplace's equation depend on and reach their extrema on the boundary values of $\mathbf{u}$. For simple geometry, as will be shown in the next section, the solution for $u_x(x)$ is linear with x, a fact that is assumed to be true in most step-compression elastographic imaging experiments.

III. PROPOSED TECHNIQUES FOR ESTIMATING ELASTIC PROPERTIES OF TISSUES

A. Step-compression imaging

For convenience we consider a two-dimensional case of a linear viscoelastic, homogeneous, isotropic material with tissue mimicking properties: E_0 in the kPa range, ρ (density) near 1.0 g/cm^3, and ν (Poisson's ratio) in the range $0.49 < \nu < 0.5$, that is, nearly incompressible. This block of tissue-mimicking material is of a rectangular cross section and is rigidly constrained along one face and further constrained by a parallel plate used for compression or other enforced displacements. We further assume that the tissue mimicking material is allowed to slip freely along the two constraining plates so that the displacement and stress fields will be independent of position in the y direction. Body forces due to gravity are assumed to be negligible. The example is shown in Fig. 1.

We assume that compression is applied at time t_0, and that images are obtained using some ideal imaging system, before and after the compression step. In the case of viscoelastic or poroelastic materials, the state of the material response and its image will be time dependent until sufficient relaxation has occurred. Assuming that a dense field of displacements can be estimated from the two images, in the homogeneous case, Eq. (11) predicts that the displacement $u_x(x)$ will be linear with x, as shown in Fig. 1(b) (solid lines). In the case where a small inhomogeneous region of $E' > E_0$ (assumed here to be of relatively small contrast $E'/E_0 < 2$), is present, a plot of displacement taken on a line bisecting the inhomogeneity will produce a local deviation from the linear slope. The exact details depend on the precise geometry and the stress concentration effect,[34] but the general trend is shown in Fig. 1(b) (dotted lines).

Although the presence of the inhomogeneity can be detected from inspection of the displacement estimates (assuming reasonable elastic contrast and very high imaging signal to noise), it is convenient to display a strain image, $\epsilon_{xx} = du_x/dx$, as this produces a more intuitive result. Homogeneous regions undergo constant strain in this example, and hard inclusions result in locally reduced strain, except for stress concentration effects that are localized near the boundaries. This is demonstrated graphically in Fig. 1(c). The terms elastography and elastographic imaging generally refer to strain images produced in this way. As long as the overall stress produced by the compression is approximately constant over the imaging region, the strain image values will correlate with local relative values of E.

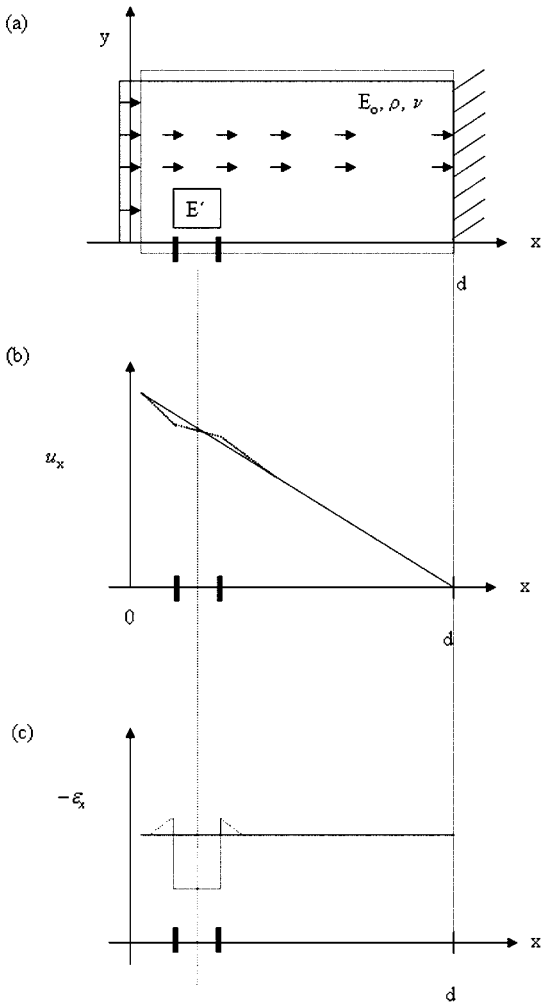

FIG. 1. Schematic of static compresson experiment on a rectangular block of viscoelastic material constrained at position d, containg a small block of material. The larger block has Young's modulus E_0, density, ρ, and Poisson's ratio, ν, while the smaller block has an elevated Young's modulus $E' < 2E_0$. (a) Block before (solid lines) and after (dotted lines) compression in the positive x direction by a rigid plate. (b) General trend of the resulting displacement field (u_x; vertical axis) along a line parallel to the x-axis through the small rectangular inclusion. (c) Strain field ($-\epsilon_x$; vertical axis) along this same line. The dotted lines indicate the perturbation caused by the presence of the inhomogeneity.

B. Shear step imaging

As an alternative to a single compression step, one can apply a single shear step, obtaining images before and after the deformation with some suitable imaging system. The displacement information is similar to that gained by compression, as shown in Fig. 2. Barbone and colleagues have shown[17] that the shear experiment creates a result that is

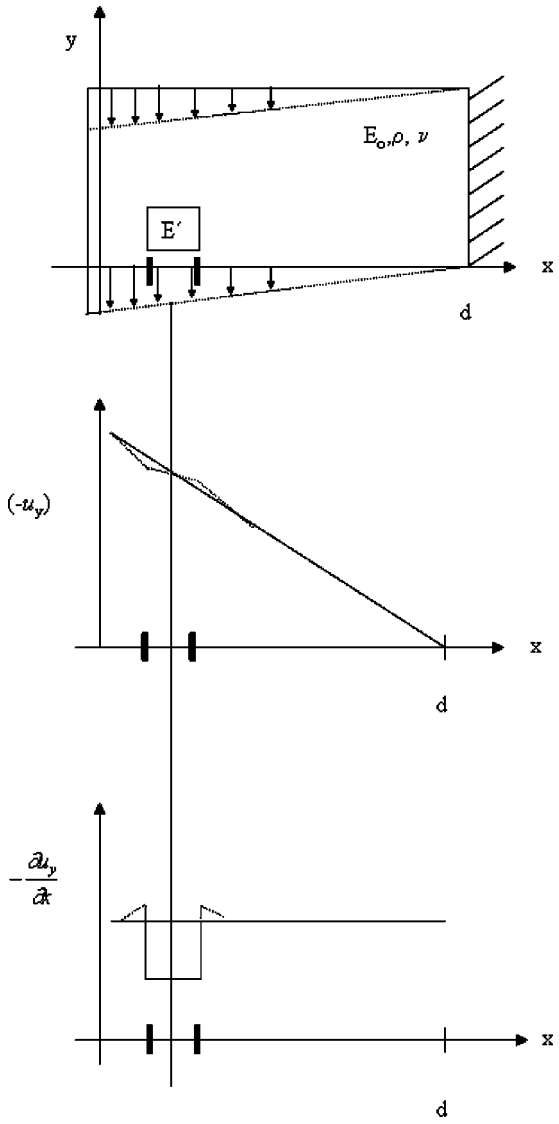

FIG. 2. Static shear experiment on a same block shown in Fig. 1: (a) Block before (solid lines) and after (dotted lines) shear by a rigid plate. (b) Shear displacement field (u_y; vertical axis) along a line parallel to the x-axis through the small rectangular inclusion. (c) Shear strain field along this same line. The dotted lines indicate the perturbation caused by the presence of the inhomogeneity.

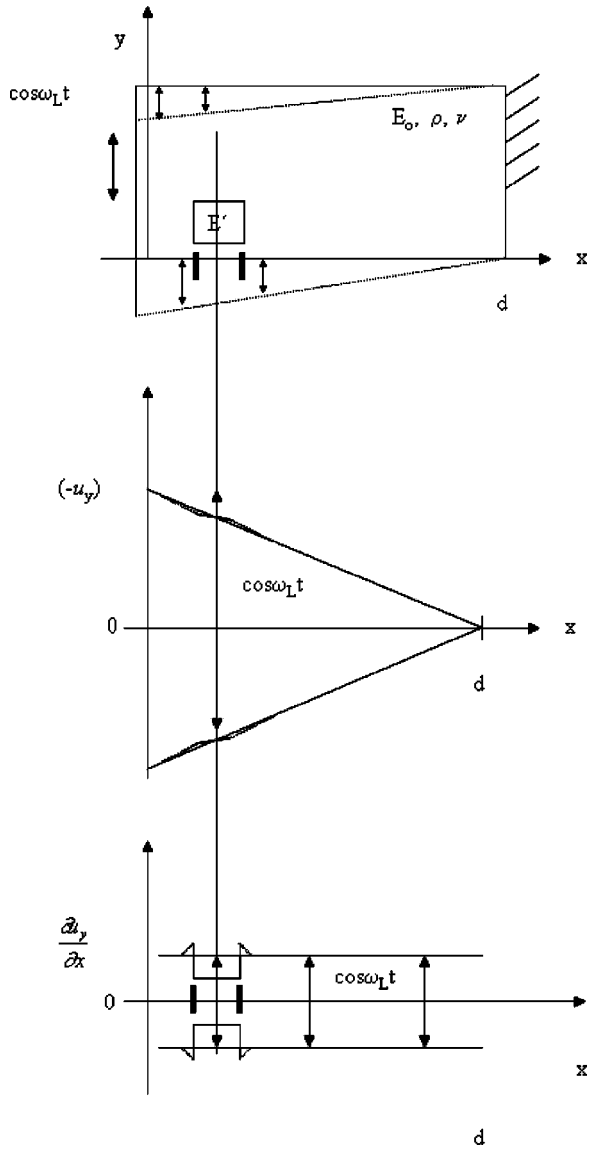

FIG. 3. Cyclical quasi-static shear experiment on the block shown of Fig. 1: (a) Block before (solid lines) and at peak (dotted lines) shear. The applied shear is sinusoidal at low frequency. (b) Peak shear displacements (solid line), along a parallel to the x-axis through the small rectangular inclusion, are linear but slowly time-varying. (c) Peak shear strain along this line is also slowly time-varying. The dotted lines indicate the perturbation caused by the presence of inhomogeneity.

complementary to the compression result when one considers the uniqueness of inverse solutions from these experiments. However, the details of that subject are beyond the scope of this discussion. As in the compression step results, Eq. (11) predicts that for a homogeneous medium displacement, $u_y(x)$ will be linear with x, which can be perturbed by an inclusion. As before, the exact details of the shear in the vicinity of the inclusion require treatment of the exact geometry and elastic contrast of the inclusion. However, stress concentration effects are highly localized in the surrounding medium. As demonstrated in Fig. 2, a spatial derivative can be employed to produce a more intuitive display where homogeneous regions exhibit constant shear strain, $\epsilon_{xy}=(1/2)[\partial u_y/\partial x+\partial u_x/\partial y]$. However, it must be understood that constant strain image values correlate with constant E only under certain idealized, low-contrast conditions.

C. Cyclic, quasistatic imaging

If a shear step is repeated sinusoidally at a relatively slow rate (e.g., at less than five cycles per second), then for most practical cases of tissues and organs, the inertial terms of the governing equations can still be neglected. The behavior can be described in the same functional form as the static case, but modified by the addition of a sinusoidal time-varying term. Thus, if the shear plate of Fig. 2 is moved as $u_y(x=0)=U_0\cos\omega_L t$, where ω_L is low frequency, then $u_y(x)=U_0(1-x/d)\cos\omega_L t$ for $0<x<d$, and the resulting strain is similarly time varying. This is shown schematically in Fig. 3. The practical advantages of cyclic quasistatic methods over single-step methods are primarily due to the ability to average and automate, thereby reducing noise and artifacts.[16,35]

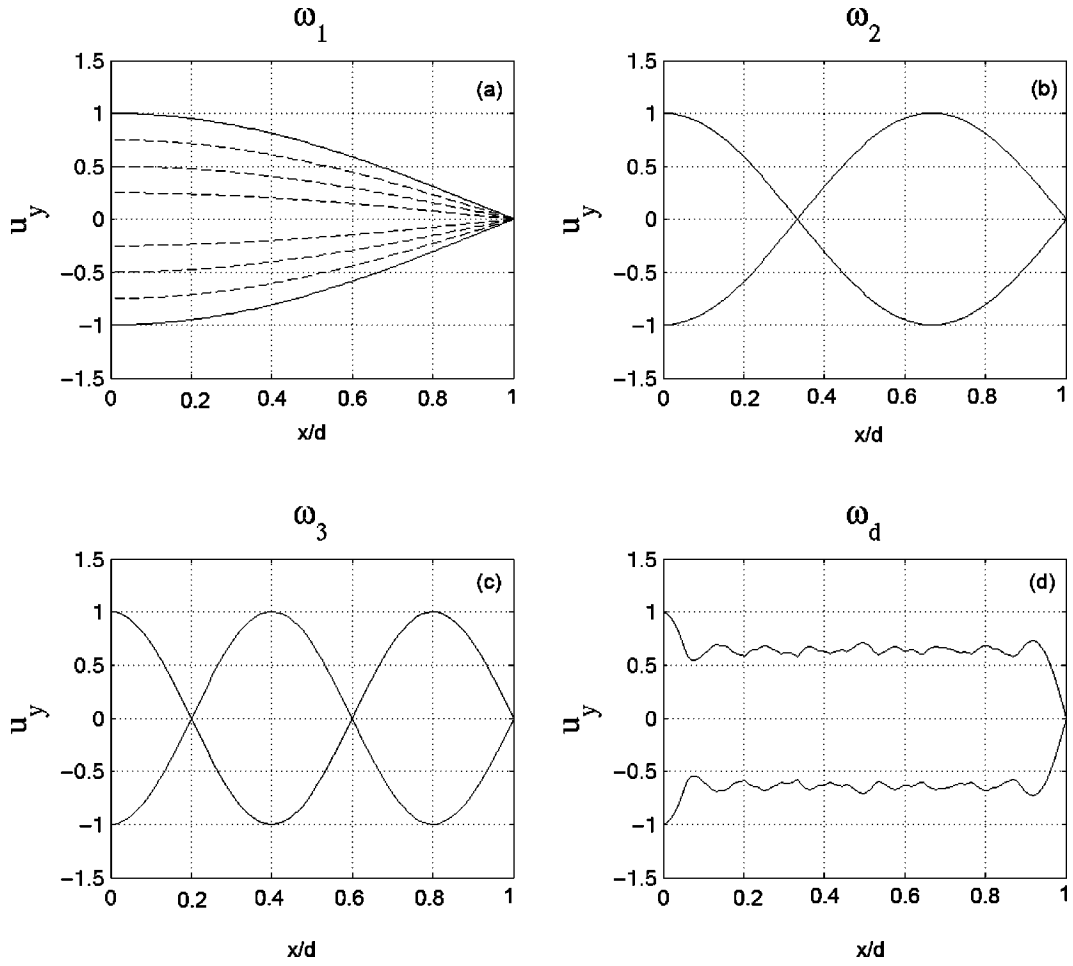

FIG. 4. Displacement fields at the block surface (see Fig. 1) during application of a sinusoidal shear with frequencies above the quasi-static range. (a) First mode. (b) Second mode. (c) Third Mode. (d) Result of many modal frequencies applied simultaneously as ''chords.''

D. Shear wave vibration

As the left vertical plate of Fig. 3 is displaced at higher frequencies, the time-varying inertial terms of the governing equation cannot be ignored and the behavior of the medium obeys the classic wave equation.

For a plane wave propagating in the x direction with particle motion in the y direction [$u_y = u_y(x,t)$ and $u_x = u_z = 0$], the shear wave equation [Eq. (7)], reduces to a one-dimensional equation of the form

$$\frac{\partial^2 u_y}{\partial x^2} = \frac{1}{c_s^2}\frac{\partial^2 u_y}{\partial t^2}. \tag{12}$$

For regular geometries and simple conditions, with low loss or attenuation, the response of the medium will peak at specific eigenfrequencies, with standing wave or eigenmodal patterns produced within the interior. Specifically, these occur when the frequency is such that odd multiples of quarter-wavelengths in the x direction are created. These frequencies are given by

$$f = \frac{2n-1}{4}\left(\frac{c_s}{d}\right), \quad \text{where}$$

$$c_s = \sqrt{\frac{E}{3\rho}}, \quad \text{the shear wave speed.}$$

In this case, we are explicitly treating the resonance as a one-dimensional problem for simplicity. For example, this would be equivalent to having the medium extend for a great length in the y axis compared to the dimension d.

The first few eigenmodes are sketched in Figs. 4(a), 4(b), and 4(c). Note the presence of nodes and antinodes within the eigenmode patterns at higher eigenfrequencies. These modal patterns are observed in regularly shaped phantoms and even in organs such as the liver at low frequencies (lowest eigenmode).[36] These eigenmode patterns can make it more difficult to visually identify regions of different elasticity.

However, the eigenmode patterns are unlikely at higher eigenfrequencies, where the irregular shape of organs, imperfect boundary conditions, and loss all conspire against modal pattern. In any event, the orthogonal nature of the successive eigenmodes makes it possible and beneficial to combine different frequencies into a multiharmonic excitation, which tends to produce a uniform vibration field, free of nulls. These multifrequency excitations are represented in Fig. 4(d), and have been referred to as ''chords.''[37] Regions of inhomogeneity would then cause variations in the vibration

patterns that can be more easily identified when using multifrequency excitations.

These vibration patterns can be imaged in real time using modified color Doppler techniques and are generally referred to as vibration sonoelastography, or simply, sonoelastography. Specifically, the Doppler spectral variance has been shown to be proportional to the vibration displacement amplitude in a sinusoidal steady state.[38] This can be displayed as a color scale overlay on the B-scan image. It has been shown by theory, by finite element modeling, and by experiments that hard inclusions present as a void or local reduction in the vibration pattern.[9] These are illustrated in Fig. 5. In this example of sonoelastography, it is not necessary to take a spatial derivative, particularly in the case where more uniform vibration patterns have been formed in the background. However, in the case where lower frequencies are employed, a derivative operation can be useful to enhance the detectability of lesions.[8]

E. Transient elastography

Transient elastography utilizes a short tone burst of vibration. This can be related to sinusoidal steady-state excitation by the use of Fourier transform relations. However, in transient experiments the forward propagating wave can be resolved and analyzed separately from the reflected waves, and this can be advantageous in some situations. In either case, the effect of an inhomogeneity is governed by the elastic-Born approximation[9] for those cases where the inhomogeneity has limited elastic contrast with respect to the surrounding background medium.

F. Detectability and resolution of issues

Of great concern in the lesion detection problem is the practical limit on the detectability of a low elastic contrast, small lesion in tissue, and the resolvability of multiple discrete small lesions. We assume in this discussion a high signal-to-noise ratio within the displacement field estimates such that derivative operations are practical and we further assume that background uniformity is nearly ideal.

For strain imaging, the general concept has already been introduced: after a derivative operation on the displacement estimations, hard inclusions will be displayed as a local region of lower strain, surrounded by localized stress concentration effects in many cases. However, it is clear from the sequence of operations that a hard inclusion must be larger than the resolution scale of the imaging system. Otherwise, it is not possible to estimate displacements, and then spatial derivatives of displacements, that fall exclusively within the inclusion. If this is satisfied, and ignoring any stress concentration effects, the strain contrast $\epsilon_{xx}(\text{lesion})/\epsilon_{xx}(\text{background})$ is directly proportional to $E_0(\text{background})/E'(\text{lesion})$, the inherent elastic contrast. The resolvability of multiple inclusions as discrete small lesions is similarly tied to the imaging system resolution plus any localized effects of stress concentration. In practice, additional practical considerations of noise, decorrelation, and displacement estimates, all complicate the issue of contrast.[39]

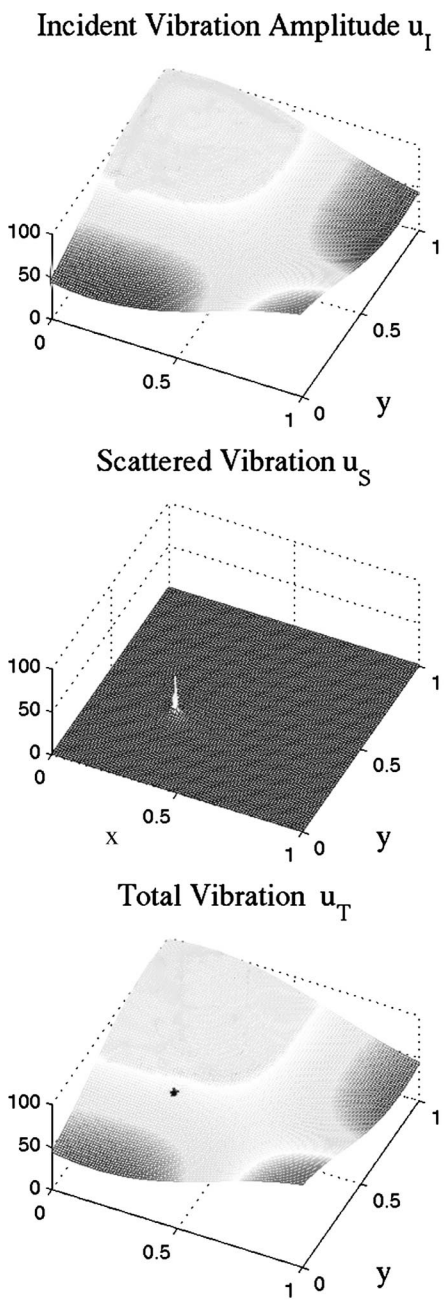

FIG. 5. Detectability and point spread function for a subresolvable elastic inhomogeneity. (top) Incident peak vibration amplitude field in a 2D region containing a small inhomogeneity with Young's modulus $E'>E_0$. (middle) The vibration field resulting from scattering by the inhomogeneity. (bottom) Total observed vibration which is the sum of a and b.

For shear wave excitation in sonoelastography and MRE, the detectability and resolution issues are recast as wave phenomena. The incident shear wave must satisfy the shear wave equation [Eq. (7)]. In the elastic-Born approximation[9] a small elastic inhomogeneity at position x' acts as a source of a scattered shear wave, and the strength of this source is proportional to the elastic contrast, $(E'-E_0)/E'$, times the wave number squared, times the strength of the incident shear wave A:

$$\nabla^2\mathbf{u}+k^2\mathbf{u}=Ak^2\left(\frac{E'-E_0}{E'}\right)\delta(\vec{x}-x'). \tag{13}$$

Within the elastic-Born approximation, the resulting so-

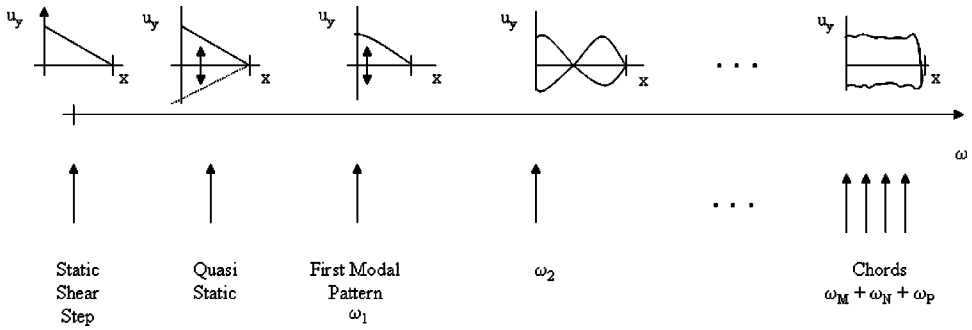

FIG. 6. Summary image showing the continuum from step displacement through dynamic vibration and multiple tones. The displacement field u_y is given in each case. The solution for displacement in homogenous object is linear for the static case, sinusoidal for modal patterns at eigen-frequencies, and approaches a constant for multiple, simultaneous ''chord'' excitation.

noelastic vibration image will be comprised of the addition of a homogeneous solution to Eq. (13) (right-hand side equal to zero) plus the scattered wave. This is depicted in Fig. 5.

Conceptually, this means that even a very small point inhomogeneity, even one well below the resolution of the imaging system, can be detected as a localized disturbance in the form of a free space Green's function, that is a $1/r$ falloff, as depicted in Fig. 5. This is similar to a small point source of light detected (and then blurred) by an optical imaging system, even though the point source aperture may be below the nominal resolution of the imaging lens. However, the strength of the inhomogeneity's signature increases with increasing frequency. Simulations and experiments have demonstrated that the sonoelastic image contrast of lesions increases with increasing frequency[8] until other frequency-dependent effects, such as lossy behavior, present a practical upper frequency limitation.[40]

This wave behavior limits the resolvability of two small neighboring points since the Green's function scattered waves pattern produced by each has an inherent type of blur, which will add coherently when the two points are closely spaced. Thus, no general claim for subresolution resolvability can be made, even though a general claim for subresolution detectability can be made.

IV. DISCUSSION AND CONCLUSION

A plethora of techniques for estimating and imaging the elastic properties of tissue have been proposed, each one employing a unique excitation function to create displacements in tissue. We demonstrate, however, that the most commonly utilized methods, from step-compression elastography through vibration (sono) elastography, fall on a continuum of elastic behavior. The information that can be derived from an ideal imaging system can be used, in each case, to identify an inclusion that is defined by some elastic contrast compared to the background. However, the particular details of preprocessing, detectability, and resolvability do change from static and quasistatic to dynamic systems where wave behaviors are exhibited. Figure 6 compares the shear behavior of a simple homogeneous system as it is excited by different displacement functions along the continuum of frequencies.

As a practical matter, the imaging system (typically ultrasound or MRI) resolution and noise characteristics will limit the performance of elasticity imaging and reconstruction schemes, along with the other practical limits from tissue motion and loss mechanisms. Specifically, on the static and low-frequency side of the continuum, tissue motion out-of-plane, noise, and speckle decorrelation artifacts from rotations all limit the displacement and derivative of displacement estimations.[39] At the other end of the continuum, the high losses or attenuation of shear waves above 200–400 Hz creates a practical limitation on whole organ penetration and potential increases in lesion contrast that would otherwise be predicted from Eq. (12). Lower bounds on correlation-based displacement estimates[40] and Doppler estimates of vibration amplitudes,[38] and MRE detection of vibration[23] have demonstrated very fine scale (micron or below) possibilities given an adequate signal-to-noise ratio.

There is another important topic of exact inverse solutions (of unknown elastic properties from the imaging data) that is beyond the scope of this paper. However, a few general remarks can be made. The exact inversion of static and quasistatic cyclic compression cases requires knowledge of boundary conditions that in most cases lie outside of the imaged region of interest. Solving for the unknown stress field (including localized stress concentrations) is difficult but necessary to utilize the local stress–strain behavior to solve for elastic parameters. In shear wave propagation, however, local estimates of displacement and wave behavior can be used to generate localized estimates of elastic properties, either through direct inversions or through forward iterative approaches. In all cases, the problem of noise in estimating spatial (or temporal) derivative terms can be a major limiting factor.

In this paper we have emphasized the common groundwork, and common information, that is obtainable over a wide range of experimental approaches to elastography.

ACKNOWLEDGMENTS

This work was supported in part by NIH 5 R01 AG16317-03, ''3D sonoelastography imaging for prostate cancer.''

[1] A. P. Sarvazyan, O. V. Rudenko, S. D. Swanson, L. B. Fowlkes, and S. Y. Emelianov, ''Shear wave elasticity imaging: a new ultrasonic technology of medical diagnostics,'' Ultrasound Med. Biol. **24**, 1419–1435 (1998).
[2] T. A. Krouskop, D. R. Doughtery, and S. F. Levinson, ''A pulsed Doppler ultrasonics systems for making noninvasive measurements of the me-

chanical properties of soft tissues,'' J. Rehabil. Res. Dev. **24**(2), 1–8 (1987).
[3] Y. Yamakoshi, J. Sato, and T. Sato, ''Ultrasonic imaging of internal vibrations of soft tissue under forced vibration,'' IEEE Trans. Ultrason. Ferroelectr. Freq. Control **37**, 45–53 (1990).
[4] R. M. Lerner, K. J. Parker, J. Holen, R. Gramiak, and R. C. Waag, ''Sonoelasticity: Medical elasticity images derived from ultrasound signals in mechanically vibrated targets,'' *Proceedings of the 16th International Acoustical Imaging Symposium (Plenum)*, 1988, Vol. 16, pp. 317–327.
[5] R. M. Lerner, S. R. Huang, and K. J. Parker, ''Sonoelasticity images derived from ultrasound signals in mechanically vibrated targets,'' Ultrasound Med. Biol. **16**, 231–239 (1990).
[6] K. J. Parker, S. R. Huang, R. A. Musulth, and R. M. Lerner, ''Tissue response to mechanical vibrations for 'sonoelasticity imaging','' Ultrasound Med. Biol. **16**, 241–246 (1990).
[7] L. Gao, K. J. Parker, R. M. Lerner, and S. F. Levinson, ''Imaging of the elastic properties of tissue—A review,'' Ultrasound Med. Biol. **22**, 959–977 (1996).
[8] K. J. Parker, D. Fu, S. M. Gracewski, F. Yeung, and S. F. Levinson, ''Vibration sonoleastography and the detectability of lesions,'' Ultrasound Med. Biol. **24**, 1937–1947 (1998).
[9] L. Gao, K. J. Parker, S. K. Alam, and R. M. Lerner, ''Sonoelasticity imaging: Theory and experimental verification,'' J. Acoust. Soc. Am. **97**, 3875–3880 (1995).
[10] S. F. Levinson, M. Shinaguwa, and T. Sato, ''Sonoelastic determination of human skeletal muscle elasticity,'' J. Biomech. **28**, 1145–1154 (1995).
[11] F. Yeung, S. F. Levinson, D. Fu, and K. J. Parker, ''Feature-adaptive motion tracking of ultrasound image sequences using a deformable mesh,'' IEEE Trans. Med. Imaging **17**, 945–956 (1998).
[12] J. Ophir, I. Cespedes, H. Ponnekanti, Y. Yazdi, and X. Li, ''Elastography: A quantitative method for imaging the elasticity of biological tissues,'' Ultrason. Imaging **13**, 111–134 (1991).
[13] J. Ophir, B. Garra, F. Kallel, E. Konofagou, T. Krouskop, R. Righetti, and T. Varghese, ''Elastographic imaging,'' Ultrasound Med. Biol. **26**, s23–29 (2000).
[14] R. Righetti, F. Kallel, R. J. Stafford, R. E. Price, T. A. Krouskop, J. D. Hazle, and J. Ophir, ''Elastographic characterization of HIFU-induced lesions in canine livers,'' Ultrasound Med. Biol. **25**, 1099–1113 (1999).
[15] P. Chaturvedi, M. F. Insana, and T. J. Hall, ''Ultrasonic elasticity imaging to model disease-induced changes in soft-tissue structure,'' Med. Image Anal **2**, 325–338 (1998).
[16] M. O'Donnell, A. R. Skovorada, B. M. Shapo, and S. Y. Emalianov, ''Internal displacement and strain imaging using ultrasonic speckle tracking,'' IEEE Trans. Ultrason. Ferroelectr. Freq. Control **41**, 314–325 (1994).
[17] A. Oberai, N. Gokhale, and P. E. Barbone, ''Direct reconstruction of elastic modulus images from ultrasound images'' (Abstract), *Proceedings of the 2nd International Conference on the Ultrasonic Measurement and Imaging of Tissue Elasticity*, 2003, Vol. 2, p. 69.
[18] T. J. Hall, Y. Zhu, and C. S. Spalding, ''In vivo real-time freehand palpation imaging,'' Ultrasound Med. Biol. **29**, 427–435 (2003).
[19] B. Brendel, S. Siebers, M. Scholz, C. Welp, J. Werner, A. Lorenz, A. Pesavento, and H. Ermert, ''Intraoperative applications of elasticity imaging using vibrography,'' in Ref. 17.
[20] R. Muthupillai, D. J. Lomas, P. J. Rossman, J. F. Greenleaf, A. Manduca, and R. L. Ehman, ''Magnetic resonance elastography by direct visualization of propagating acoustic strain waves,'' Science **269**, 1854–1857 (1995).
[21] R. Sinkus, J. Lorenzen, D. Schrader, M. Lorenzen, M. Dargatz, and D. Holz, ''High-resolution tensor MR elastography for breast tumour detection,'' Phys. Med. Biol. **45**, 1649–1664 (2000).
[22] M. M. Doyley, J. B. Weaver, E. E. W. VanHouten, F. E. Kennedy, and K. D. Paulsen, ''Thresholds for detecting and characterizing focal lesions using steady-state MR elastography,'' Med. Phys. **30**, 495–504 (2003).
[23] D. B. Plewes, J. Bishop, A. Samani, and J. Sciarretta, ''Visualization and quantification of breast cancer biomechanical properties with MRE,'' Phys. Med. Biol. **45**, 1591–1610 (2000).
[24] S. Catheline, F. Wu, and M. Fink, ''A solution to diffraction biases in sonoelasticity: The acoustic impulse technique,'' J. Acoust. Soc. Am. **105**, 2941–2950 (1999).
[25] L. Sandrin, S. Catheline, M. Tanter, X. Hennegin, and M. Fink, ''Time-resolved pulsed elastography with ultrafast ultrasonic imaging,'' Ultrason. Imaging **21**, 259–272 (1999).
[26] T. Sugimoto, S. Ueha, and K. Itoh, ''Tissue hardness measurement using the radiation force of focused ultrasound,'' *IEEE 1990 Ultrasonics Symposium Proceedings*, 1990, pp. 1377–1380.
[27] F. L. Lizzi, R. Muratore, C. X. Deng, J. A. Ketterling, S. K. Alam, S. Mikaelian, and A. Kalisz, ''Radiation-force technique to monitor lesions during ultrasonic therapy,'' Ultrasound Med. Biol. **29**, 1593–1605 (2003).
[28] W. F. Walker, F. J. Fernandez, and L. A. Negron, ''A method of imaging viscoelastic parameters with acoustic radiation force,'' Phys. Med. Biol. **45**, 1437–1447 (2000).
[29] K. R. Nightingale, M. L. Palmeri, R. W. Nightingale, and G. E. Trahey, ''On the feasibility of remote palpation using acoustic radiation force,'' J. Acoust. Soc. Am. **110**, 625–634 (2001).
[30] M. Fatemi and J. F. Greenleaf, ''Ultrasound-stimulated vibro-acoustic spectrograpy,'' Science **280**, 82–85 (1998).
[31] M. Fatemi and J. F. Greenleaf, ''Application of radiation force in noncontract measurements of elastic parameters,'' Ultrason. Imaging **21**, 147–154 (1999).
[32] H. Kolsky, *Stress Waves in Solids* (Dover, New York, 1963).
[33] J. D. Achenbach, *Wave Propagation in Elastic Solids* (North-Holland, Amsterdam, 1984).
[34] I. Shames, *Mechanics of Deformable Solids* (Prentice–Hall, Englewood Cliffs, NJ, 1964).
[35] M. M. Doyley, J. C. Bamber, F. Fuechsel, and N. L. Bush, ''A freehand elastographic imaging approach for clinical breast imaging: system development and performance evaluation,'' Ultrasound Med. Biol. **27**, 1347–1357 (2001).
[36] K. J. Parker and R. M. Lerner, ''Sonoelasticity of organs: Shear waves ring a bell,'' J. Ultrasound Med. **11**, 387–392 (1992).
[37] L. S. Taylor, D. J. Rubens, and K. J. Parker, ''Artifacts and artifact reduction in sonoelastography,'' *2000 IEEE Ultrasonics Symposium Proceedings*, 2000, pp. 1849–1852.
[38] S. R. Huang, R. M. Lerner, and K. J. Parker, ''On estimating the amplitude of harmonic vibrations from the Doppler spectrum of reflected signals,'' J. Acoust. Soc. Am. **88**, 310–317 (1990).
[39] Srinivusan, R. Righetti, and J. Ophir, ''Tradeoffs between axial resolution and signalto-noise ration in elastography,'' Ultrasound Med. Biol. **29**, 847–866 (2003).
[40] W. F. Walker and G. E. Trahey, ''A fundamental limit on delay estimation using partially correlated speckle signals,'' IEEE Trans. Ultrason. Ferroelectr. Freq. Control **42**, 301–308 (1995).